



## Smectite clays as the quasi-templates for platinum electrodeposition

E.K. Lavrentyeva<sup>a</sup>, S.Y. Vassiliev<sup>a</sup>, E.E. Levin<sup>a</sup>, A.A. Tsirlin<sup>b</sup>, S.N. Polyakov<sup>c</sup>, M. Leoni<sup>d</sup>, K.S. Napolskii<sup>a</sup>, O.A. Petrii<sup>a,1</sup>, G.A. Tsirlina<sup>a,\*,1</sup>

<sup>a</sup> Moscow State University, Chemical Faculty, Leninskie Gory, 1-str. 3, Moscow 119991, Russia

<sup>b</sup> Max Planck Institute for Chemical Physics of Solids, Nöthnitzer Str. 40, D-01187 Dresden, Germany

<sup>c</sup> Technological Institute for Superhard and Novel Carbon Materials, Centralnaya Street, 7a, Troitsk, Moscow region, 142190, Russia

<sup>d</sup> University of Trento, Via Mesiano 77, I-38123 Trento, Italy

### ARTICLE INFO

#### Article history:

Received 27 July 2011

Received in revised form

20 November 2011

Accepted 24 November 2011

Available online 6 December 2011

#### Keywords:

Clay

Template

Platinum

Electrodeposition

Methanol oxidation

### ABSTRACT

Smectite clays suspended in a platinum deposition solution are here shown to increase the specific surface area of electrodeposited Pt on gold and porous carbon paper supports, and to enhance the specific activity of Pt towards methanol oxidation under steady-state conditions. Organomodified natural bentonite shows a more pronounced effect with respect to natural montmorillonite and synthetic laponite. The effect of clay, as evidenced by microscopy and X-ray diffraction, is to decrease the average size of the Pt crystallites and simultaneously the degree of their mutual coalescence. This effect is associated with suppression of Pt secondary nucleation observed in deposition current transients, and the electrocatalytic activity is suggested to be affected by the intergrain boundaries.

© 2011 Elsevier Ltd. All rights reserved.

### 1. Introduction

Electrodeposited platinum catalysts can be fabricated in more controllable manner as compared to chemically reduced materials. For applications (e.g. in the context of fuel cells research), the prospects of Pt electrodeposits on smooth supports are however rather limited. Nevertheless, dispersed Pt electrodeposits attract systematic attention [1–3], because they can be used as a model system to study complex structural effects in electrocatalysis. Structural features of these materials are in fact representative for real catalysts that cannot be properly modelled by the macroscopic size single crystals or well-arranged ensembles of separate single crystalline nanoparticles.

Platinum deposits prepared from conventional electrolytes are actually the assemblies of nanocrystals having an average effective diameter of ca. 10 nm and a size distribution highly dependent on the deposition mode. These crystals hold together due to the formation of intergrain boundaries [4,5]. Some portion of the internal surface of these dispersed porous materials is screened by the boundaries, but about a half of the total true surface takes part in the interfacial electrochemical processes. Basically, the deposits (at

least those fabricated from the most usual chloride baths) demonstrate the specific surface area of several  $\text{m}^2 \text{g}^{-1}$  or higher.

Grain boundaries are certainly non-equilibrium structural features of electrodeposits. The same features can be observed also in carbon-supported catalysts when the metal loading is high. On the other hand, high loading is recognized today as the preferable (at least for fuel cell catalysts). For electrodeposited samples, the grain boundaries are created in the course of secondary nucleation of Pt on freshly formed surface of primary nuclei (initially deposited crystals).

Our recent studies of Pt [5] and PtRu [6] have already confirmed that, under some circumstances, the catalytic activity of dispersed metals towards the oxidation of methanol and CO correlates with the amount of grain boundaries. It is therefore clear that an optimisation of the grain boundary should lead to the control of catalytic activity. However, it is difficult to vary the quantity of grain boundaries without affecting crystal size and lattice defects that, in turn, influence the catalytic activity as well. Those three interrelated features are usually controlled by a single parameter, the deposition potential.

In order to understand the structural complexity of electrodeposited Pt, it is highly desirable to vary the content of grain boundaries over a broad range keeping the same deposition potential. This is what we want to accomplish in this study with the use of a quasi-templating procedure. The quasi-templating approach was worked out earlier for the Pd-poly(ethylene glycol) [7,8] and

\* Corresponding author. Tel.: +7 495 9391321; fax: +7 495 9328846.

E-mail address: [tsir@elch.chem.msu.ru](mailto:tsir@elch.chem.msu.ru) (G.A. Tsirlina).

<sup>1</sup> ISE member.

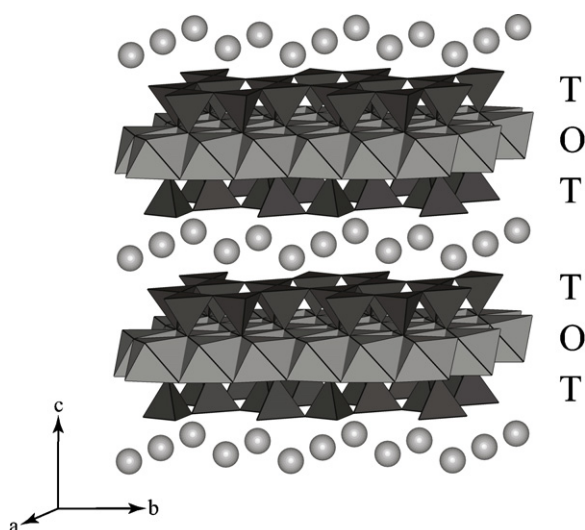


**Fig. 1.** The crystal structure of the smectite clay. T and O denote the layers of silicate tetrahedra and aluminium (magnesium) octahedra, respectively; circles show the exchangeable cations accommodated in the interlayer space.

the Pt-dodecatungstate [9] systems. Quasi-templating is based on the effect of strongly adsorbing substances on the mutual location and ordering of growing nanocrystals. In quasi-templated electrodeposits, the mean crystallite size and/or the degree of surface screening by grain boundaries tend to decrease as compared to non-templated deposits formed at the same potential. Compared to non-templated deposits, a higher specific surface area can be achieved for the same size distribution.

Our hypothesis (qualitative at this stage) on the quasi-templating effect consists in the suppression of the growth of Pt crystallites by large templating molecules. We assume that the templating agent should not be necessarily dissolved; the same role can be played by colloid particles immobilized on the freshly formed deposit surface. Electrocrystallization-accompanied electrophoretic deposition of colloid particles is a wide research area (see e.g. [10,11]), but silicate and aluminosilicate colloid modifiers are only scarcely studied [12].

Some clays, zeolites and various oxohydrated silicates have been previously used as the additives to plating solutions [13,14] or in the form of gel containing the discharging metal ion [15]. Various types of metal dispersions were obtained due to the effects of the colloidal medium on the diffusion of the reagent and the specific bonding of metal ions to the particles in suspension.

Our choice of smectite clays as a templating agent is motivated by their stability in acids and their general chemical inertness that can avoid the risk of Pt poisoning and catalyst degradation. Smectites are layered aluminosilicates with a general formula  $\text{Si}_x(\text{Al}/\text{Mg})_y\text{O}_p(\text{OH})_q$ . They have a 2:1 layered structure with a single layer of  $\text{AlO}_6(\text{MgO}_6)$  octahedra (Fig. 1, O-layers) sandwiched in between two layers of silicate tetrahedra (Fig. 1, T-layers).<sup>2</sup> A variety of smectites results from Al(Mg) substitution in the O-layers and/or Si in the T-layers by lower-charged cations. The substitution results in excess of electrons in the layers [17] that is compensated by loosely bound exchangeable cations located in the interlayer space (Fig. 1). Clay particles suspended in aqueous medium are usually aggregates of several platelets arranged parallel to each other, with a nanometer range periodicity.

When clay platelets are captured by the growing metal deposit, there is a chance to increase the electrocatalytic activity due to bifunctionality. The latter is known for clay-supported metals (intercalated clay catalysts) applied in heterogeneous catalysis [18,19]: bifunctional Pt-intercalated clay catalysts are commonly used for the hydrogenation of aldehydes [20] and alkynes [21], and sometimes demonstrate a synergetic increase in the activity [20,22]. Catalytic sites of clays are Lewis and Brønsted acid centers [23] located at the edges and surfaces of clay platelets, or formed by hydrated exchangeable cations. Despite all clays are insulating, a lot of examples of clay-modified electrodes (CME) can be found, especially in electroanalysis and in molecular recognition applications [24–26]. CME conductivity results from the permeability of clay for small molecular/ionic species and by fast proton transport along the water-hydroxide net. However, some aspects of the CME electrochemistry remain unclear, especially those related to the electron transfer mechanism: for instance an electron-hopping mechanism is widely accepted for zeolite-containing electrodes [27,28].

Smectite clays are here used as a suspension added to the platinum deposition bath. The clay particles in these suspensions are expected to be 30–50 nm long and a few nm thick [29–31], i.e. of a size comparable with that of Pt nanocrystals in the electrodeposits (5–20 nm [1]). To establish the effect of clays on the properties of the Pt electrodeposit, we compared the influence of three different smectites, namely Laponite (Lap), Montmorillonite (Mont) and Bentonite (Bent), on the structure of the Pt deposits. Lap is a single-phase synthetic clay that closely resembles the natural clay hectorite, Mont is a purified natural montmorillonite clay, and Bent is a natural montmorillonite modified with an organic component to improve the stability of clay suspensions in water [32].

## 2. Experimental

Electrodeposition of Pt and electrochemical measurements were carried out at 25 °C with an EG&G potentiostat PARC 273 in a three-electrode cell. The counter electrode was a Pt foil, and the reference electrode was a saturated calomel electrode (SCE) connected to the cell via a Luggin capillary. Hereinafter, the potentials  $E$  are given versus RHE ( $E_{\text{SCE}} - E_{\text{RHE}} = 0.247 \text{ V}$  in aqueous solution of 0.5 M  $\text{H}_2\text{SO}_4$ ).

Samples of polycrystalline gold foil (0.2 mm thick, 2 cm<sup>2</sup>) and carbon paper (~0.19 mm thick, 2 cm<sup>2</sup>; Toray Industries, Inc.) were used as supports. Prior to electrodeposition, the gold foils were etched in hot aqua regia for 5 s to obtain a reproducible surface state. The carbon paper supports were used without any pretreatment. Platinum was electroplated from aqueous solutions 0.01 M  $\text{Na}_2\text{PtCl}_6 + 0.02 \text{ M HCl}$  and from clay suspensions of 0.2, 0.5 and 1 wt.% in this solution. The suspensions were mixed with a magnetic stirrer in closed flasks for 2, 3 and 6 h, respectively. An Ocean Optics spectrophotometer was used to control the concentration of hexachloroplatinate in the deposition solutions. Unless otherwise noted, all samples specified as Pt/clay refer to those deposited from the 0.2 wt.% suspensions. The electrodeposition of Pt was performed at constant potentials  $E_d = 100 \text{ mV}$  and 250 mV. The total charge  $Q_d$  spent for electrodeposition was always 2C for gold supports; for all the deposits on carbon paper supports, the values are tabulated below. The weight of Pt in the samples was close to 1 mg (for Au support) and to 3 mg (for carbon paper support), therefore the accuracy of Pt weighting hardly exceeded 20%. An averaged mass of 5–6 samples for each type of deposit was employed to estimate the specific surface areas of Pt( $S(\text{C})$ ) and the current efficiency.

True surface area  $S_H$  of electrodeposited Pt and Pt/clay samples was determined coulometrically from the hydrogen desorption region of cyclic voltammograms (CV) measured at 0.1 V s<sup>-1</sup> within the potential range of 0.06–1.24 V in a 0.5 M  $\text{H}_2\text{SO}_4$  solution

<sup>2</sup> Images were obtained using the VESTA software [16].

deaerated with Ar for 1 h. The potential was cycled until a stationary voltammogram was obtained (usually in the fiftieth cycle). The surface area of all freshly deposited samples was determined prior to the structural analysis. For prolonged ageing experiments, the samples were cycled at  $0.02 \text{ V s}^{-1}$  in the potential range of 0.06–1.4 V.

Steady-state polarization curves were measured in 0.1 M  $\text{CH}_3\text{OH} + 0.5 \text{ M H}_2\text{SO}_4$  under potentiostatic mode; the current was considered stationary if its further change with time was less than 0.7% per minute.

To prepare the plating bath, MilliQ water,  $\text{Na}_2\text{PtCl}_6$  (Merc, GR for analysis),  $\text{H}_2\text{SO}_4$  (Merc, GR for analysis), HCl (Merc, GR for analysis),  $\text{CH}_3\text{OH}$  (distilled), Montmorillonite (Cloisite®  $\text{Na}^+$ , Southern Clay Products, Inc.), Bentonite (Fluka Chemika-BioChemika Corp.) and Laponite (Laponite RD, Conservation Resources INT'L LLC.) were used.

STM imaging was carried out *ex situ* with an “Umka” instrument (“NanoIndustry”, Moscow), using  $-0.3 \text{ V}$  bias and tunneling currents up to 0.5 nA (no effects of bias sign were observed). Pt–Ir STM probes were sharpened by mechanical cutting of Pt–Ir wire (10 wt.% Ir). To construct size distributions, six images of  $120 \times 120$ – $180 \text{ nm} \times 180 \text{ nm}$  size obtained from two identical samples of each type of the deposit were used, with about 50–120 isolated particles visualized in each image. Submicron-resolution scanning electron microscopy was performed using both a LEO Supra 50 VP (Carl Zeiss, Germany) and a JEOL JSM6380 (Jeol, Japan) instrument equipped with INCA 250 EDS (Oxford Instruments, UK) analysis module. TEM imaging was carried out with a digital LEO 912 AB (Carl Zeiss, Germany) microscope.

X-ray powder diffraction (XRD) data for Pt electrodeposits were collected in step-scan mode at room temperature using a  $\theta$ – $2\theta$  Bragg–Brentano RIGAKU D/max RC diffractometer operating with  $\text{CuK}_\alpha$  radiation and equipped with a graphite analyser and a scintillation detector. XRD patterns were recorded in the  $2.6$ – $140^\circ$  range of  $2\theta$  with a step of  $0.02^\circ$ . For phase identification, the ICDD PDF-2 database [33] was used. The instrumental line profile broadening effects were measured on the NIST SRM660a ( $\text{LaB}_6$ ) standard. Microstructural analysis (crystallites size distribution in terms of coherently scattering domains, dislocation density and stacking faults concentration calculations), was done within the framework of the Whole Powder Pattern Modelling (WPPM) approach [34] using the PM2K software package [35].

The Philips PW2400 X-ray fluorescence spectrometer (INEOS RAS, Moscow) was used for the chemical analysis of the clays when no data from the manufacturer were available. A Netzsch STA 449 PC instrument was used for the TG-DTA analysis of Mont and Bent: thermal decomposition products were monitored online using a Netzsch QMS 403C mass spectrometer. In this analysis, a 112 mg sample of Bent was heated up to  $900^\circ\text{C}$  ( $10^\circ\text{C min}^{-1}$ ) in oxygen flow ( $40 \text{ ml min}^{-1}$ ). Additionally, we investigated the organic stabilizer contained in the Bent sample by liquid chromatography (Shimadzu LC-2010A) and Raman spectroscopy (Raman RXN1 Systems, Kaiser Optical Systems, Inc.). To extract the stabilizer, Bent was mixed in a proportion 1:100 with carbon tetrachloride (for liquid chromatography) or water (for Raman spectroscopy), and kept at room temperature for three days under slow stirring. Before the measurements, the clay particles were separated by centrifugation.

### 3. Results and discussion

#### 3.1. Clays characterization

The complete characterization of clay samples is complicated by their possible multi-phase nature and the flexibility of chemical composition. The XRD patterns of all three clays (Fig. 2) show the features typical of layered systems (diffraction bands), although the

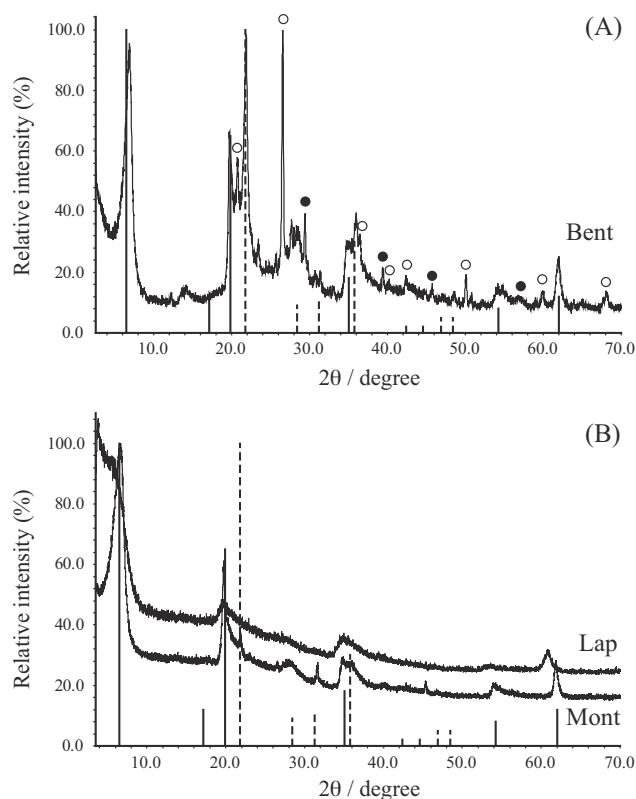


**Fig. 2.** XRD patterns of Bent (A) and Mont, Lap (B). Solid vertical lines show the reflections of Mont [33] (#29-1498). Dashed vertical lines, solid circles, and open circles indicate impurities in the Bent sample: opal [33] (#38-448), calcite [33] (#72-1937), and quartz [33] (#46-1045), respectively.

shapes and intensities of the reflections are somewhat different for Mont, Lap and Bent due to the difference in their chemical composition and microstructure. For Bent, additional reflections are found, indicating the presence of opal (#38-448), quartz (#46-1045) and calcite (#72-1937) as impurities.<sup>3</sup> All these impurities are typical for bentonite as a natural multi-phase material [36]. The ambiguity in chemical composition and the irregular shape of the reflections prevented us from a quantitative phase analysis. A rough estimate using the strongest reflections yields 30–60 wt.% of the smectite-type phase in the Bent sample. The Mont sample contains a small amount of opal, while Lap is free from crystalline impurities.

Chemical composition of the clays (Table 1) is more complex for Mont and Bent as compared to Lap. According to TG-DTA, Bent and Mont samples contain, respectively, ca. 20 and ca. 2 wt.% of organic substances, while in Lap only traces of organic contaminations are found. Unfortunately, the composition of the organic stabilizer in Bent is not provided by the manufacturer. According to our Raman spectroscopy and chromatography investigation, this stabilizer consists mostly of aromatic compounds. Mass spectroscopy in the course of TG-DTA measurements confirms thermal decomposition of these compounds with the formation of hydrocarbons and carbon dioxide. Correspondingly, in what follows, one should keep in mind the possible influence of organic substances on the deposition of Pt templated with Bent.

To estimate the size of clay fragments in suspension, we put a drop of the aqueous suspension (0.1 wt.%) on a highly oriented pyrolytic graphite (HOPG) substrate. We were able to observe some aggregates (Fig. 3) even in the *ex situ* STM configuration: the

<sup>3</sup> The numbers provided in parentheses are those of the corresponding card in the ICDD PDF-2 database [33].

**Table 1**  
Chemical composition of clays (wt.%).

Clay	Na <sub>2</sub> O	MgO	Al <sub>2</sub> O <sub>3</sub>	SiO <sub>2</sub>	P <sub>2</sub> O <sub>5</sub>	S	K <sub>2</sub> O	CaO	TiO <sub>2</sub>	Fe <sub>2</sub> O <sub>3</sub>	LiO <sub>2</sub>	Li <sup>a</sup>
Mont	5.61	1.05	17.36	56.74	0.03	0.32	0.07	1.73	0.12	4.43	–	13.14
Bent	6.35	1.11	9.07	43.75	0.24	0.20	0.81	1.62	0.27	1.05	–	35.43
Lap <sup>b</sup>	2.8	27.5	–	59.5	–	–	–	–	–	–	0.8	8.2

<sup>a</sup> Losses on ignition (for Mont and Bent were determined at 950 °C).

<sup>b</sup> [www.laponite.com](http://www.laponite.com)

natural moisture in the tunneling gap may indeed facilitate the imaging of insulating fragments (in this case, as the STM device operates like a Scanning ElectroChemical Microscope, SECM [37,38]). The thickness of Mont particles is ca. 15 nm, and their diameter is ca. 70–100 nm (Fig. 3a). Lap particles are of ca. 70 nm size and ca. 5 nm thick (Fig. 3b), even if their mean size reported by the manufacturer (<http://www.laponite.com>) is significantly lower (ca. 25 and 1 nm, respectively). Most likely, we cannot resolve some boundaries between individual particles in the aggregates immobilized on HOPG, so the above values for Mont and Lap can be overestimated. Characteristic size of Bent particles (typically rectangular) is 40–60 nm, and the thickness is ca. 10 nm (Fig. 3c). This is in agreement with more detailed studies reported e.g. in Refs. [31,39]. Opal, a component of Bent, is a partly amorphous phase of hydrated silica formed by cristobalite-like network of SiO<sub>4</sub> tetrahedra. This network is three-dimensional, but different shapes (fibrous, plate-like) of opal microcrystals have been reported (see [40] and references therein). Therefore, an assignment of the imaged particles from Bent suspension to a certain phase remains somewhat ambiguous.

### 3.2. Electrodeposition

Experimental transients for Pt and Pt/clay deposition at  $E_d = 250$  mV on Au are shown in Fig. 4A. Despite the pronounced scatter of current values, some tendencies in transients' behavior are well reproducible in all the experiments. For deposition from Bent- and Mont-containing suspensions, the current remains lower than for clay-free solutions and the suspensions of Lap. Bent and Mont affect the shape of the transients as well: the decrease in current at the initial period (0–100 s) appears to be less sharp; when approaching the plateau region (>300 s), the current starts to decrease sharper. The lowest currents were observed for Mont suspensions.

We should stress that no pronounced effect of the deposition potential on the current value is observed in the absence of Bent, while in Bent-containing medium the current at  $E_d = 250$  mV is significantly lower during the whole deposition period than the current at  $E_d = 100$  mV (compare Fig. 4A and B). Clay effect on the transient shape is less pronounced at  $E_d = 100$  mV compared to  $E_d = 250$  mV; in the former case, no current decrease during the initial period (0–160 s) is observed (Fig. 4B).

Spectrophotometry demonstrates that clays suspended in the deposition solution do not lead to any decrease in the concentration of the hexachloroplatinate anion. This means that the “clay effect” on the nucleation-growth rate is hardly induced by complexing of the hexachloroplatinate anion with the functional groups at the surface of clay particles. Electrostatic reasons look more plausible. Although the potential of zero free charge (pzfc) was not evaluated precisely for solutions under investigation, this value can be estimated as ca. 220 mV by taking into account the pH-dependence of pzfc [41,42]. Therefore, at  $E_d = 250$  mV the free charge of platinum surface is already positive, and electrostatic adsorption of clay should be expected, thus inducing the screening of newly formed growing surface. In contrast, electrodeposition at 100 mV obviously takes place at the negatively charged support, and no clays can be

attached electrostatically. An example for the Pt/Bent system at 100 mV (Fig. 4B) demonstrates a less pronounced inhibition than at  $E_d = 250$  mV. Here, we also have to consider the effect of the organic stabilizer equally adsorbing at both 100 and 250 mV. The adsorption of organic molecules will result in additional screening of the growing surface. However, when comparing the Bent and Mont systems, we found no correlation between the deposition kinetics and the amount of organic component, although Bent contains ten times more organic component than Mont (Fig. 4A).

Another phenomenon, which can accompany electrodeposition, is the electrophoretic movement of the negatively charged clay particles from the cathode where Pt deposition occurs. A rough estimate based on Smoluchowski equation [43] and typical zeta potential of smectite clays (ca. 10 mV in suspensions at pH ~ 2 and the same ionic strength as for the deposition solution under investigation [44,45]) yields 10 nm s<sup>-1</sup> rate of electroporetic movement. As soon as this value is comparable with the rate of the deposit growth, the mechanical capture of the clay particles by the growing deposit is surely possible.

Current efficiency determined gravimetrically is 70–100% (see discussion in Ref. [1]), but the accuracy of these values is fairly low because of the low deposit thickness (200–250 nm). Within this accuracy, no systematic effect of clay on current efficiency was found.

### 3.3. True surface area

The voltammograms of Pt and Pt/clay samples deposited at 250 mV (for equal geometric areas and deposition charge) are given in Fig. 5A. Independently of deposition potential (Fig. 5b, Table 2), the presence of clay in the deposition solutions leads to an increase in  $S_H$  as determined from hydrogen desorption with identical double layer correction. Owing to the inaccuracy of the weighting procedure, the accuracy of the recalculated specific surface area  $S(C)$  is much lower than that of  $S_H$ . However, the increase in  $S(C)$  due to the Bent and Mont addition (Table 2) exceeds the possible error of few m<sup>2</sup> g<sup>-1</sup>. In contrast to the Pt/Bent sample, Pt/Mont and Pt/Lap samples show a pronounced difference in the shape of the hydrogen desorption region of voltammograms (as compared to typical Pt deposits): the relative height of the second peak is reduced, and both peaks are shifted to lower potentials (Fig. 5A).

Among Pt/clay samples, Pt/Bent demonstrates the highest specific surface area, while Pt/Lap is similar to usual Pt deposits (Fig. 5A, Table 2). In the former, one cannot exclude an additional effect of the organic stabilizer, as some organic surfactants are known to support platinum nanostructuring [46–49]. Additional experiments were performed in order to check for the possible templating effect of the organic stabilizers dissolved in the deposition solution. First, the suspension of Bent in the same portion of Milli-Q water was prepared three times, with a subsequent separation of the precipitate by centrifugation. Each time a new portion of Bent was suspended to achieve a higher concentration of the stabilizer in water. Then two deposition solutions were prepared: (a) by adding Na<sub>2</sub>PtCl<sub>6</sub> into water separated from washed Bent, and (b) by suspending washed Bent in the usual platinum plating solution. These experiments confirmed that organic stabilizers can increase the

**Table 2**  
True surfaces ( $S_H$ ) and specific surfaces  $S(C)$ , determined coulometrically from the hydrogen desorption region of CV;  $S(\text{STM})$  and degree of coalescence calculated from STM data for Pt and Pt/clay samples deposited on Au. Total charge spent for electrodeposition ( $Q_d$ ) was 2 C for all samples.

Sample	$S_H$ (cm <sup>2</sup> )	$S(C)^a$ (m <sup>2</sup> g <sup>-1</sup> )	$S(\text{STM})$ (m <sup>2</sup> g <sup>-1</sup> )	Degree of coalescence, 1- $S/S(\text{STM})$
Pt ( $E_d = 250$ mV)	92 ± 8	13.0 ± 4.8	22 ± 2	0.41 ± 0.27
Pt/Mont ( $E_d = 250$ mV)	122 ± 2	17.5 ± 5.3	24 ± 0	0.27 ± 0.22
Pt/Bent ( $E_d = 250$ mV)	151 ± 8	21.6 ± 7.3	24 ± 0	0.10 ± 0.30
Pt/Lap ( $E_d = 250$ mV)	98 ± 0	14.0 ± 4.0	22 ± 0	0.36 ± 0.18
Pt ( $E_d = 250$ mV) control experiment (see text)	125 ± 3	18.0 ± 5.6	–	–
Pt ( $E_d = 100$ mV)	105 ± 13	11.6 ± 4.0	23.5 ± 0.5	0.51 ± 0.12
Pt/Bent ( $E_d = 100$ mV)	157 ± 17	15.7 ± 4.8	24 ± 0	0.35 ± 0.13

<sup>a</sup>  $S(C)$  is normalized per the average mass of 5–6 samples.

specific surface area of Pt. However, their effect is less pronounced than the effect of non-washed Bent in suspension, despite of much higher concentration of the organic substances in the deposition solution (a). The specific surface area obtained in these control experiments does not exceed 18 m<sup>2</sup> g<sup>-1</sup>, whereas for Pt/Bent it is clearly above 20 m<sup>2</sup> g<sup>-1</sup> (Table 2). In the control experiment (b), no templating effect was observed. This is not surprising, because the suspension of washed Bent is unstable (it precipitates in ca. 10 min).

Since not only organically modified Bent, but also Mont (with much lower content of organic substances) increases the specific surface area of Pt deposits (Table 2), the templating effect can not be attributed only to the presence of the organic additives in the Bent suspension. We conclude that, at least for Bent, templating is induced by both clay and stabilizer in parallel. The presence of the latter can be risky for Pt catalytic activity, as organic molecules could strongly adsorb on the active sites of the catalysts and act as a poison. Fortunately, our voltammetric experiments with Pt foil in 0.5 M H<sub>2</sub>SO<sub>4</sub> containing suspended clays demonstrate a slightly distorted hydrogen adsorption region, but satisfactory purity of the surface is easily achieved by using the conventional cycling pretreatment (usually in the fiftieth cycle). This means that the presence of the organic stabilizer in Bent is not detrimental for the catalytic activity.

Actually, the increase in the specific surface area is rather typical for template-assisted deposits [7,9]. To propose a more controllable quasi-templating procedure, it is important to understand whether such an increase results from smaller size of Pt crystals, from lower degree of coalescence, or from both factors simultaneously. To clarify the problem, the results of SEM, STM and XRD characterization of deposits are discussed below.

### 3.4. Morphology

SEM images of Pt/Bent samples deposited on Au (Fig. 6) clearly show that the adhesion of Pt/Bent deposited at 250 mV (Fig. 6B) is weaker as compared to samples deposited at 100 mV (Fig. 6E) as well as to usual Pt deposited at the same potential (Fig. 6A). All these images differ qualitatively from the images of Au support reported earlier [4,5]. The appearance of cracks gives indirect evidence of a lower coalescence of the Pt particles in the Pt/Bent samples deposited at 250 mV, and/or of the relaxation of high residual stresses previously present in the deposit. Despite the morphology of our thin deposits is still strongly affected by the roughness of the etched gold support, it is possible to recognize a more distinct globular microstructure for Pt/Bent (Fig. 6E) than for Pt (Fig. 6D) at  $E_d = 100$  mV.

Microanalysis (EDX) failed to discover any appreciable quantities of Si or other clay-related chemical elements inside the platinum deposits. The presence of clay inclusions (huge Bent aggregates) was confirmed only for higher Bent content in the plating

solution (Fig. 6C). Si-containing inclusions remained visible even after a thorough washing of the samples under ultrasonic stirring, thus indicating that the clay was strongly attached to the Pt deposit.

Since the resolution of the SEM images is still too low to visualize separate Pt crystals, we applied *ex situ* STM. Despite of a small (and unavoidable) drift, resulting in the apparent egg-shape, particle size can be reliably determined from cross-sections. Mutual location of the particles can be determined from this data as well. Figs. 7 and 8 present Pt and Pt/clay images and corresponding size distributions of the Pt particles.<sup>4</sup> Samples deposited at  $E_d = 250$  mV and 100 mV are compared in Figs. 7 and 8. Like usual Pt deposits [1], Pt/clay materials consist of nm-size crystals. No STM features indicating the presence of clay particles are found.

As a first approximation, we fitted all distributions using lognormal functions, and determined the mean particle size ( $D$ ) (Table 3). These  $D$  values were used to estimate the weight of Pt corresponding to the formation of one monolayer of Pt particles, and corresponding deposition charge. The latter was compared to the time dependence of the experimental deposition charge obtained by integrating the curves in Fig. 4. We found that, for all samples, the hypothetical first monolayer of Pt particles can be formed during the first 30–50 s of deposition (this time range is shown by dashed vertical lines in Fig. 4). The primary nucleation maximum should surely precede the completion of the monolayer of primary crystals. Moreover, secondary nucleation always starts before a complete monolayer of primary Pt crystals is formed. Therefore, broad maxima at the deposition current transients cannot be assigned to primary nucleation, and traditional nucleation models should not be applied in this case. The most pronounced and reproducible clay effect on the deposition kinetics (current decrease after the maximum) should be discussed in the context of secondary nucleation exclusively. A comparison of transients normalized per current maxima demonstrates that current growth is much stronger in the absence of clays (Fig. 4C). For pure Pt samples, when ca. 4–5 effective monolayers of Pt particles are deposited, the current changes only slightly (this region can be already solidly assigned to repeated secondary nucleation events). Contrary, for Pt/Bent sample the current decrease is systematically observed as the number of effective monolayers of Pt particles increases. Deposition potential demonstrates no influence on the current in the initial region for both types of samples. This inhibitory effect of clays is independent of  $E_d$ , so we assume that it can be related only to mechanical capture of the clay particles by the growing deposit.

Size distributions (Figs. 7 and 8) demonstrate two effects of quasi-templating with clay. First, for  $E_d = 250$  mV the distribution

<sup>4</sup> We hope that the resolution of STM makes it possible to visualize separate single crystalline Pt particles, this possibility was demonstrated in Ref. [50].

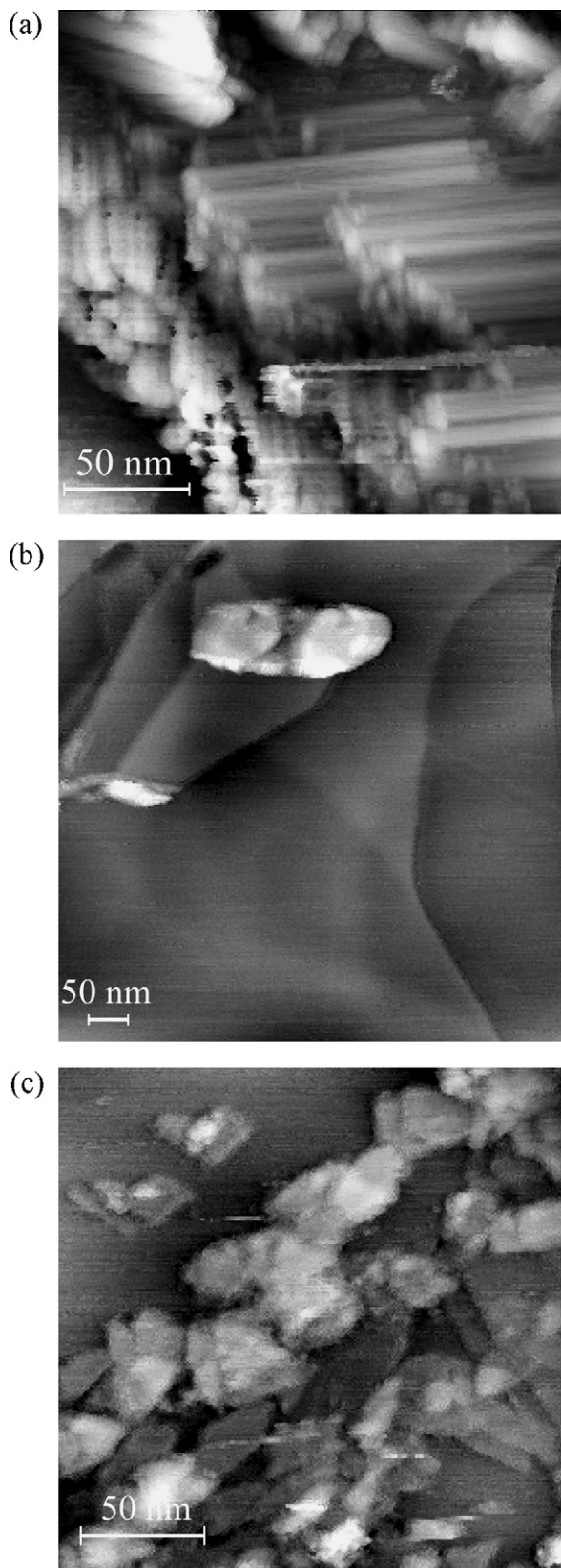


**Fig. 3.** STM images of highly oriented pyrolytic graphite with the clays immobilized from aqueous suspensions of Mont (a), Lap (b) and Bent (c). The concentration of clay in suspensions is 0.1 wt.%.

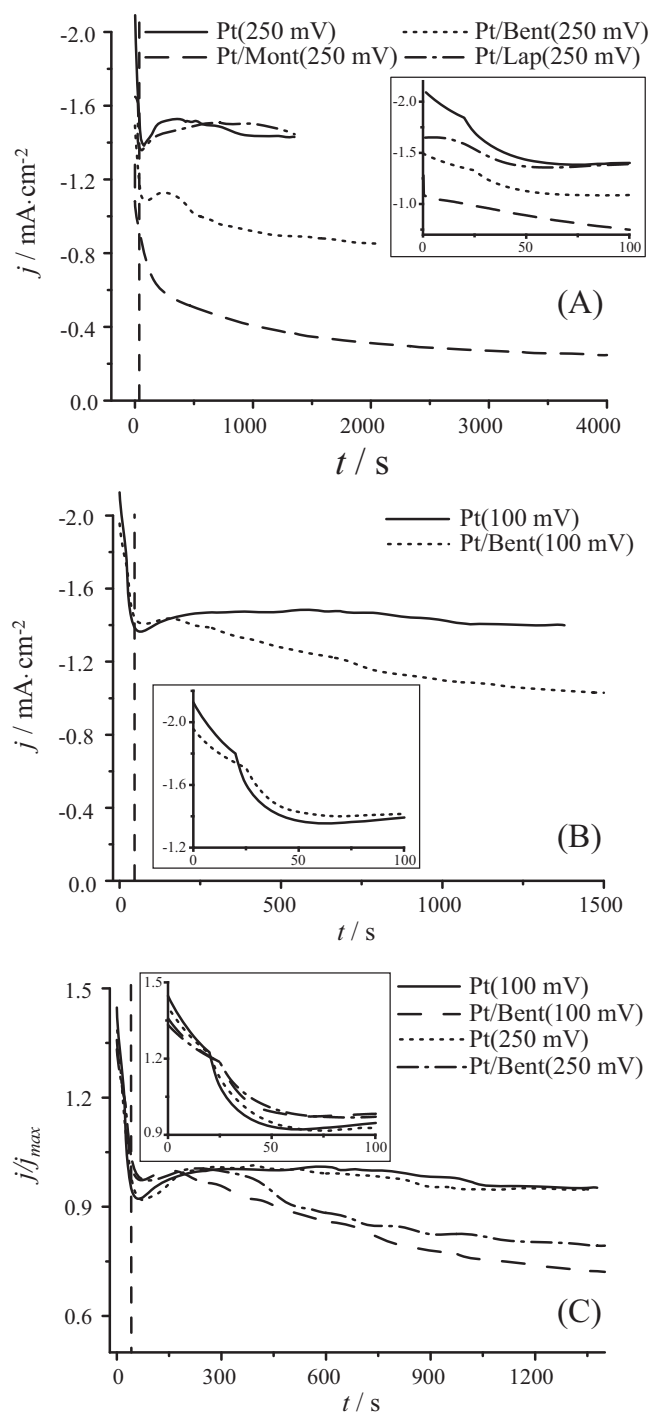


**Fig. 4.** Comparison of deposition current transients measured on Au electrode in 0.01 M Na<sub>2</sub>PtCl<sub>6</sub> + 0.02 M HCl solution (Pt) and in clay suspensions in this solution (Pt/Mont, Pt/Bent and Pt/Lap). Deposition potential (mV vs. RHE) is indicated in parentheses: 250 mV (A) and 100 mV (B). Plot (C) demonstrates deposition transients for Pt and Pt/Bent normalized per the current value in transient maximum. Vertical dashed line corresponds to the hypothetical formation of one monolayer of crystals of ca. 10 nm size, as estimated from STM and XRD data for Pt deposits. Insets: magnified intervals of  $t = 0-100$  s.

becomes more narrow (particles of diameter exceeding 17 nm disappear (Fig. 7b–d) as compared to the distribution for pure Pt deposited in the absence of clay (Fig. 7a). The effect is more pronounced for Pt/Bent and Pt/Mont and is minimal for Pt/Lap. Second, for the Pt/Bent sample deposited at  $E_d = 100$  mV (Fig. 8b) the

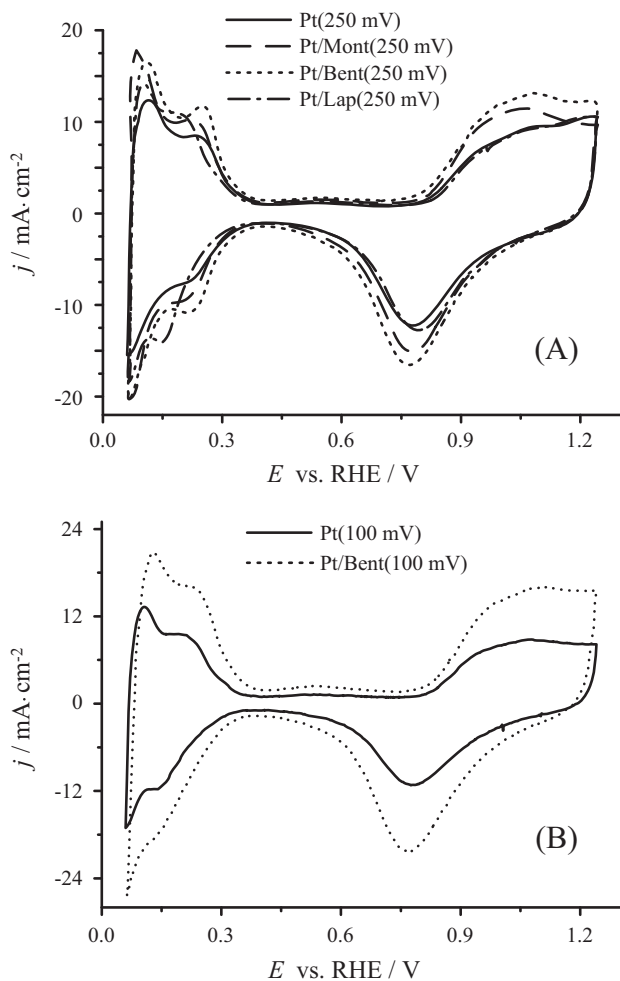


**Fig. 5.** CVs of Pt and Pt/clay samples. Deposition potential (mV vs. RHE) is indicated in parentheses: 250 mV (A) and 100 mV (B).

maximum of the distribution shifts towards smaller particle sizes as compared to pure Pt (Fig. 8a).

Using the experimental size distributions, we can also estimate the degree of coalescence of the Pt particles. The expected specific surface area  $S(\text{STM})$  is calculated under an assumption of zero coalescence, i.e. assuming that the whole surface of all the particles is accessible. Thus,  $S(\text{STM})$  is the sum of the surface area of all particles normalized per their total weight. This value is compared to the experimental  $S(\text{C})$ : when  $S(\text{C})/S(\text{STM})$  approaches 1, the degree of coalescence tends to zero. Using this approach, we found that Bent and Mont decrease the degree of coalescence in Pt deposits, while Lap does not affect this value significantly (Table 2).

In contrast to Pt samples, a significant effect of the deposition potential on the degree of coalescence is observed for Pt/Bent samples: Pt particles deposited at  $E_d = 100$  mV are more coalesced than those deposited at  $E_d = 250$  mV (Table 2). The decrease in the coalescence should be attributed to a smaller overlap of the secondary nucleation centers. This finding agrees with our assumption that electrostatic adsorption is more pronounced at  $E_d = 250$  mV.

Coalescence degrees of 0.3/0.7 are typical for Pt electrodeposits [5], while the value for Pt/Bent ( $E_d = 250$  mV) is anomalously low (Table 2) and corresponds formally to the lack of any coalescence. This value does not certainly look realistic, as the deposit is hardly stable without the grain boundaries. However,  $S(\text{STM})$  values could be underestimated if the size of some particles is overestimated (due to non-zero curvature radius of the STM probe). It may be difficult to identify the boundaries between coalesced crystals in some

of the particles by means of STM. This unavoidable underestimation is confirmed independently by XRD data.

### 3.5. XRD characterization

The XRD patterns of the Pt deposits clearly show just the peaks of Au and Pt (Fig. 9). No traces of aluminosilicate or silicate phases were found, despite the patterns were registered starting from  $2\theta \sim 3^\circ$ . According to Ref. [51], the reflections of clay appear for electrochemically deposited clay films when the thickness is above  $\sim 25$  nm. The content of clay mixed with Pt to be detectable by XRD, estimated using the PowderCell software [52] and the RIR technique [53], is quite high (ca. 10 wt.%). Therefore, our XRD data do not exclude the presence of clay in the composite deposits.

In order to quantify the lattice defects in the Pt deposits, we applied the WPPM technique which performs a microstructure analysis from powder diffraction data on the basis of physically-grounded models of the material [34]. We assumed that diffraction line profile broadening results from three factors, namely, the small crystallite size and the presence of dislocations and stacking faults. For comparison with STM data, we assumed Pt domains being spherical and showing a lognormal distribution of sizes. The microstructural parameters extracted from the data were: mean crystallite size  $D$  (XRD) and variance of the lognormal distribution [54], dislocation density  $\rho_{\text{disl}}$ , deformation fault  $\alpha$  and twin fault  $\beta$  probabilities.

The lattice parameters  $a(\text{Pt})$  are slightly different for the samples under investigation (Table 3). However, the accuracy of these values can be lower than specified in Table 3 in terms of the formal statistical error from the least-squares refinement. We assume the real precision to be  $0.01 \text{ \AA}$ , thus the deviation of the cell parameters from the bulk value ( $a_{\text{bulk}}(\text{Pt}) = 3.9231 \text{ \AA}$  (PDF2# 4-802)) is marginal and can be hardly considered as a signature of lattice compression that was previously found in Pt electrodeposits fabricated at higher potentials [5].

The results of the WPPM analysis demonstrate that Bent has the most pronounced effect of on the microstructure of Pt deposits, as it causes a decrease in crystallite size and an increase in dislocations density, as compared to the samples deposited from Bent-free solutions. We should note that for Pt/Bent and Pt (250 mV) samples  $D$  (XRD) is significantly lower than  $D$  (STM). For other clays, the specific microstructural features are less pronounced, and  $D$  (XRD) approaches  $D$  (STM). Variance is always lower for templated samples, and this decrease is more pronounced at  $E_d = 250$  mV (like other  $E_d$  effects mentioned above).

The calculated values of  $\rho_{\text{disl}}$  are similar to those frequently observed in severely deformed metals [55] or oxide materials [56]. The clays generally increase  $\rho_{\text{disl}}$  (with Pt/Mont sample being a reproducible exception), and simultaneously decrease the probability of deformation faults.<sup>5</sup> Thus, the templating with clays not only increases or decreases the defectiveness of the system, but also induces a redistribution of various types of defects. XRD data demonstrate that Lap also affects the microstructure of deposited Pt, although its effect on the surface area and deposition kinetics could not be discerned.

Unfortunately, the present analysis of the XRD data does not give any detailed information concerning intergrain boundaries that represent highly disordered regions of the sample and marginally contribute to XRD patterns. However, the observed dislocation density can be due to grain boundaries that, basically are macroscopic defects for the system.

<sup>5</sup> We should bear in mind that PM2K utilizes the formalism of Warren to evaluate the stacking faults concentration, and therefore results are meaningful only for low concentrations (below 5–10%).

**Table 3**

Cell parameters and averaged crystallite sizes for XRD patterns of Pt and Pt/clay samples deposited on Au,  $D$  (XRD) (lognormal mean) and variance (distribution half-width), dislocation density  $\rho_{\text{dist}}$ , deformation fault  $\alpha$  and twin fault  $\beta$  probabilities.  $D$  (STM) values are listed for comparison.

Sample	$a$ (Pt), Å	$D$ (XRD), nm	Variance (XRD), nm	$\rho_{\text{dist}}$ ( $\times 10^{-16}$ , $\text{m}^{-2}$ )	$\alpha$ (%) $\beta$ (%)	$D$ (STM), nm
Pt ( $E_d = 250$ mV)	$3.9197 \pm 0.0001$	$8.6 \pm 0.6$	$4.3 \pm 0.3$	$4.00 \pm 0.01$	1.8 0	11.7
Pt/Mont ( $E_d = 250$ mV)	$3.9168 \pm 0.0002$	$13.1 \pm 0.4$	$3.9 \pm 0.1$	$3.30 \pm 0.01$	0.8 0	11.7
Pt/Bent ( $E_d = 250$ mV)	$3.9186 \pm 0.0001$	$7.1 \pm 0.4$	$2.8 \pm 0.1$	$4.78 \pm 0.01$	0 0	11.3
Pt/Lap ( $E_d = 250$ mV)	$3.9213 \pm 0.0001$	$11.7 \pm 0.8$	$3.1 \pm 0.2$	$4.41 \pm 0.05$	0.3 0	12.1
Pt ( $E_d = 100$ mV)	$3.9149 \pm 0.0001$	$11.8 \pm 0.7$	$3.6 \pm 0.2$	$4.42 \pm 0.01$	0.7 0	10.8
Pt/Bent ( $E_d = 100$ mV)	$3.9151 \pm 0.0001$	$7.0 \pm 0.3$	$3.4 \pm 0.1$	$7.35 \pm 0.01$	0.6 0.6	10.2

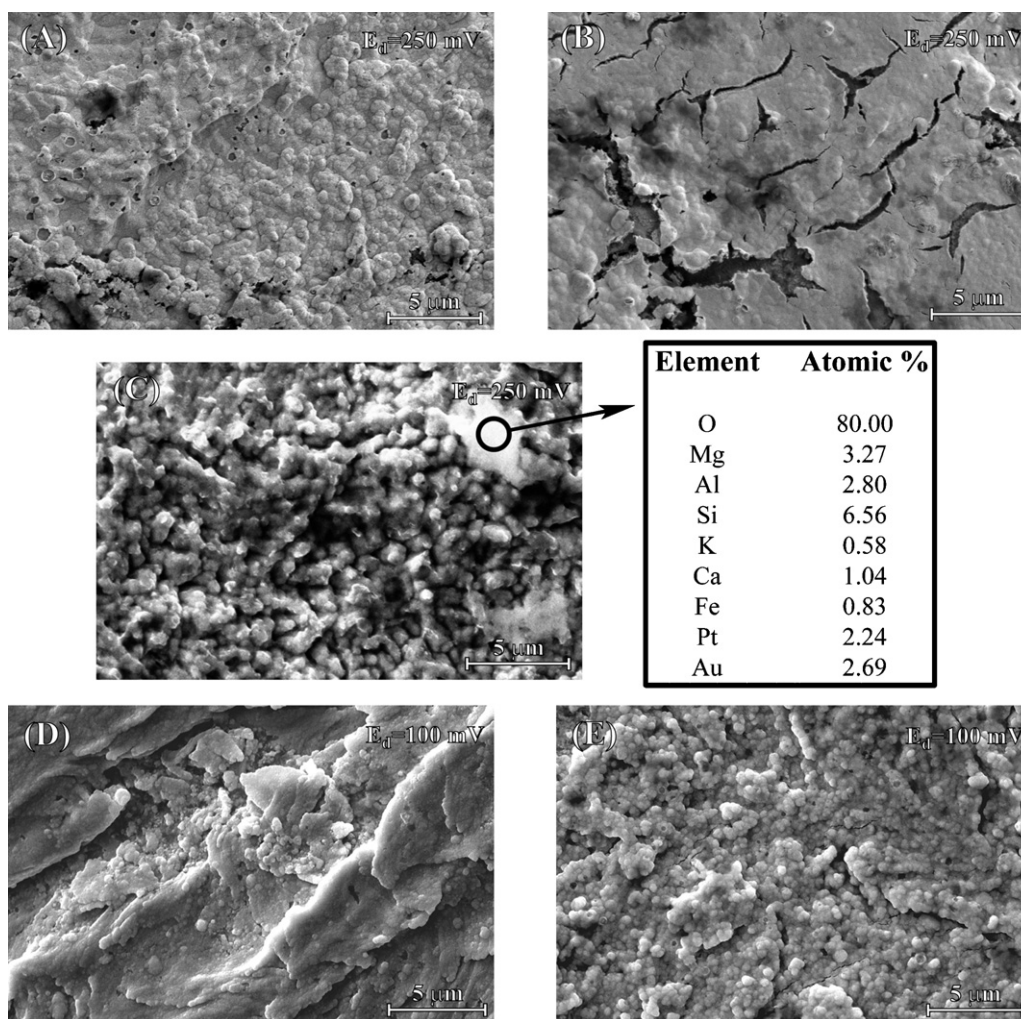


**Fig. 6.** SEM images of Pt (A and D) and Pt/Bent (B, C and E) samples. Deposition potential (mV vs. RHE) is indicated in each photo. (C) SEM and local analysis data for Pt/0.5 wt.% Bent sample (i.e., higher Bent content as compared to usual 0.2 wt.%).

### 3.6. Possible nature of clay effect on Pt dispersity

Based on the experimental data, we conclude that the clay in the deposition solution can template platinum in at least three ways:

- (i) it screens some active centers of the Au support, and therefore it decreases the number of contacts between the deposit and the support, resulting in lower adhesion;
- (ii) it decreases the growth rate of secondary Pt crystallites;

- (iii) it prevents the neighboring nanoparticles of Pt from coalescence in the course of deposition, especially at  $E_d = 250$  mV; this hypothesis is confirmed by our analysis of the  $S(C)/S(\text{STM})$  ratios.

Point (iii) can be easily understood in terms of the screening of some nucleation centers even without any appreciable effect on the secondary nucleation rate constant. Otherwise, one is unable to explain the decrease in the mean crystal size evidenced above.

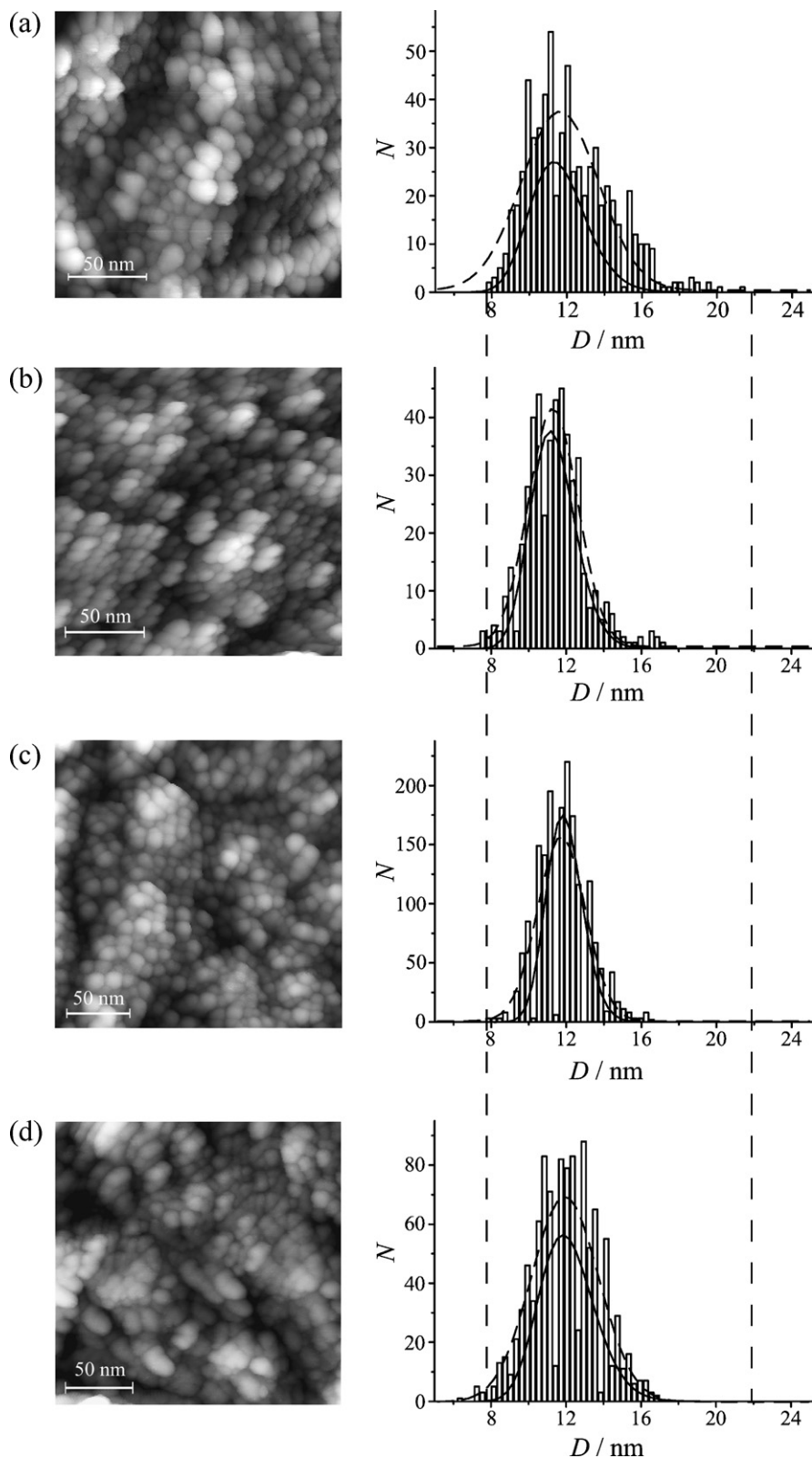


**Fig. 7.** Typical STM images of Pt (a), Pt/Bent (b), Pt/Mont (c) and Pt/Lap (d) samples deposited at  $E_d = 250$  mV and the size distributions for corresponding samples (constructed using the data from at least six images). The distributions are approximated by Gauss (dashed lines) and LogNormal (solid lines) functions. Vertical dashed lines are guides for the comparison of size distributions.

These results allow us to conclude that the electrostatic adsorption and the mechanical capture of the clay particles by the growing deposit are the key reasons for the templating effect of clays. The former phenomenon is affected by the electrode free charge

(deposition potential) and by the platelet charge. The latter depends on concentration, size and charge of clay particles, because it is regulated by an electrophoretic withdrawal of clay particles from the cathode. In the case of the organoclay Bent, the additional

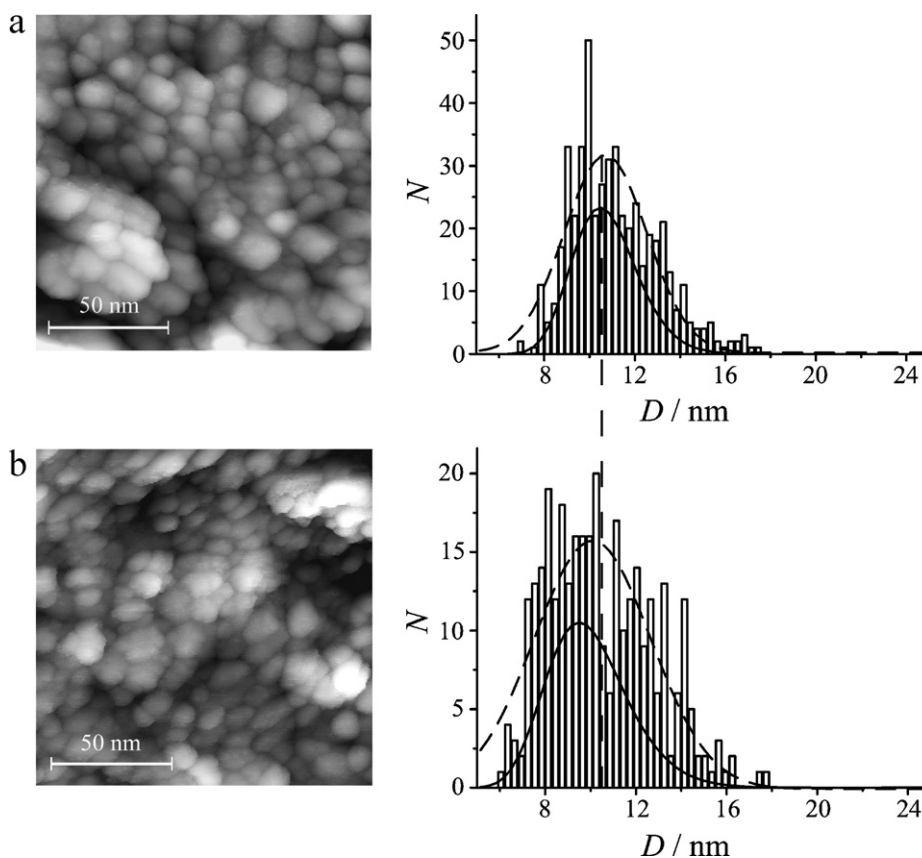


**Fig. 8.** Typical STM images of Pt (a) and Pt/Bent (b) samples deposited at  $E_d = 100$  mV and size distributions for these samples (constructed using the data from at least six images). The distributions are approximated by Gauss (dashed lines) and LogNormal (solid lines) functions. Vertical dashed lines are guides for the comparison of size distributions.

adsorption of organic stabilizer could also affect the templating process.

### 3.7. Carbon supported Pt/clay catalysts

Carbon-supported Pt electrocatalysts are extensively used in practice [57–59]. To test the applicability of the clay as a templating additive for the fabrication of this type of catalysts, we deposited Pt/Bent samples on porous carbon paper (CP). These samples are named below CP.Pt/Bent, whereas pure Pt deposits prepared for comparison are named CP.Pt.

Since the majority of typical carbon-supported catalysts contain 20–40 wt.% of Pt, we studied a model CP.Pt/Bent material with ca. 30 wt.% metal loading. The samples were deposited at  $E_d = 250$  mV.

The porous carbon paper, as well as most carbon supports, is expected to provide a lower concentration of nucleation centers than the Au supports [60]. The true surface of the porous CP support exceeds considerably its geometric area, but the material is more or less hydrophobic, and electrolyte penetration into the pores is incomplete. Deposition transients obtained for this complex electrode material demonstrate worse reproducibility as compared to the deposition on Au, but the basic qualitative tendencies of the clay templating effect can be formulated and compared with the trends described above.

The presence of Bent in the deposition solution reduces the rate of electrodeposition on CP (Fig. 10A), similar to the effect found for Au (Fig. 4A). In the majority of transients, the onset of the “plateau” region is observed earlier for the deposition from the Bent suspension than from the clay-free solution. At this stage, we assume that the components of Bent block not only nucleation centers at the external and internal surface of the CP paper, but also some narrow

pores. The latter blocking is occasional and results in lower reproducibility. The deposition current on CP is 10 times higher than on Au with the same geometric area, i.e. a lot of Pt is deposited on the internal surface. Besides, the region of the current growth is longer for CP, and the growth is sharper. We cannot exclude that the increase in the internal surface accessible for the electrochemical process takes place in the course of the deposition due to the gradual increase of hydrophilicity of CP.

The voltammograms of CP.Pt and CP.Pt/Bent samples are presented in Fig. 10B. The deposition from Bent suspensions results in the formation of deposits with higher specific surface area as compared to CP.Pt samples. The effect is similar to the deposits on Au (compare Tables 2 and 4).

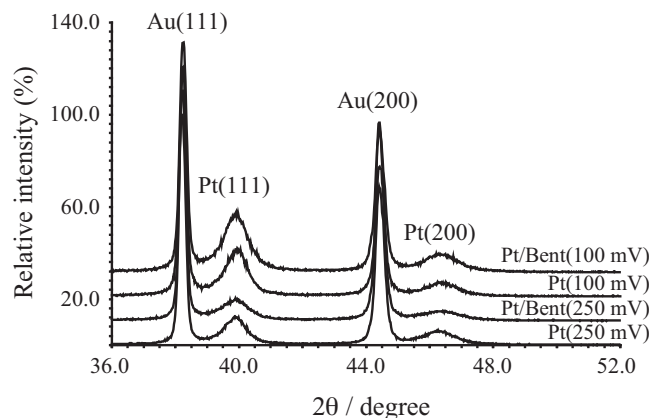


**Fig. 9.** XRD patterns for Pt and Pt/Bent deposits. Deposition potential (mV vs. RHE) is indicated in parentheses.

**Table 4**  
Total charge spent for electrodeposition ( $Q_d$ ); true surfaces ( $S_H$ ) and specific surfaces  $S(C)$ , determined coulometrically from the hydrogen desorption region of CV; degree of coalescence calculated from STM and TEM data and microstructural parameters<sup>a</sup> calculated from XRD patterns of Pt and Pt/clay samples deposited on CP at  $E_d = 250$  mV.

Sample	$Q_d$ (C)	$S_H$ (cm <sup>2</sup> )	$S(C)^a$ m <sup>2</sup> g <sup>-1</sup>	Degree of coalescence, 1-S/S(TEM)	Degree of coalescence, 1-S/S(STM)	$a$ (Pt), Å	$D$ (XRD), nm	Variance (XRD), nm	$\rho_{\text{disl}}$ ( $\times 10^{-16}$ , m <sup>-2</sup> )	$\alpha$ (%) $\beta$ (%)
CP.Pt	33	251	7.2 ± 0.4	0.87 ± 0.01	0.68 ± 0.04	3.9191 ± 0.0001	15.1 ± 0.04	3.4 ± 0.1	3.77 ± 0.01	1.2 0
CP.Pt/Bent	26	356	12.7 ± 0.9	0.77 ± 0.02	0.36 ± 0.08	3.9207 ± 0.0001	10.7 ± 0.03	4.6 ± 0.1	3.68 ± 0.01	0.8 0.8

<sup>a</sup> See notations in the title of Table 3.

As CP allows an easy detaching of fragments, it was possible to use TEM in addition to STM for a microscopic investigation of the deposits. The TEM data mainly show the internal surface, while STM visualizes the external surface. Therefore, the mean particle size  $D$  (STM) differs significantly from  $D$  (TEM). Treating the data for all fragments of nonuniform deposits on CP, we conclude that the template-assisted deposition yields a lower degree of Pt coalescence (Table 4) than for deposits on Au (compare Tables 2 and 4). However, our Pt deposits on Au are much thinner than on CP.

$D$  (XRD) values confirm that the addition of Bent in the deposition solution decreases the size of the Pt crystallites (Table 4), like

in the case of deposition on Au. The pure Pt deposits on CP show lower values of dislocation density and faulting probability as compared to the sample deposited on Au at the same potential (compare Tables 2 and 4 for  $E_d = 250$  mV). This less pronounced imperfection can be related to the higher deposit thickness and, correspondingly, to a weaker effect of the lattice mismatch between the support and deposit. However, the general effect of Bent on the microstructure (redistribution of various imperfections) remains the same as found for Au.

At this stage, we can suggest that for the samples deposited on CP the mechanical capture of the clay particles by the growing deposit is the only reasonable explanation for the templating effect of clay. However, the porosity of carbon paper can limit clay penetration and complicate the capture of clay platelets by the growing deposit. In contrast to samples deposited on Au, the electrostatic adsorption of clays on the carbon surface in the course of primary Pt nucleation is hardly possible. Electrostatic attraction is expected to appear only in the course of the secondary nucleation and growth, when a small amount of Pt is already accumulated at the interface.

### 3.8. Pt/clay prospects for methanol electrocatalysis: activity and ageing behavior

To test the electrocatalytic prospects of the fabricated Pt/clay materials, the steady-state currents of methanol oxidation in 0.1 M CH<sub>3</sub>OH + 0.5 M H<sub>2</sub>SO<sub>4</sub> solution were measured in a narrow 540–640 mV potential region (Fig. 11). These tests assumed the comparative estimate of Pt and Pt/clay specific activity. Surely, for practical goals one should compare the methanol oxidation rates at lower potentials, but this test is difficult to arrange at this stage because of the too small surface areas of the electrodes. Despite this problem, we consider the applied tests as rather reasonable because the main kinetic features (i.e. nature of the limiting step and tendency to self-poisoning) remain the same up to ca. 0.7 V [59], and the formal kinetics (e.g. Tafel parameters for the steady-state polarization curves) determined in the interval under study are typical just for low potentials interval.

The higher specific activity in respect to methanol oxidation was found for template-assisted deposits than for pure Pt deposits on gold, independently of the deposition potential and the nature of the support. The samples deposited at  $E_d = 100$  mV demonstrate higher specific activities as compared to the samples obtained at  $E_d = 250$  mV (Fig. 11A). This agrees with earlier known tendencies [61] for Pt deposits on metallic supports. For deposits on CP, the effect looks rather small (but still positive). However, if one compares the activities per Pt weight, the difference is more evident (see  $S(C)$  values in Table 4).

Taking into account the XRD data, we can speculate that the clay-induced defects play a positive role in methanol electrocatalysis. At this stage, the only correlation we have found between the activity and the microstructure is the one with the increased dislocation density (Table 3). As dislocations measured by XRD are both those inside the grains (with possible outcrop on the surface) and those forming the grain boundaries, we cannot exclude that grain

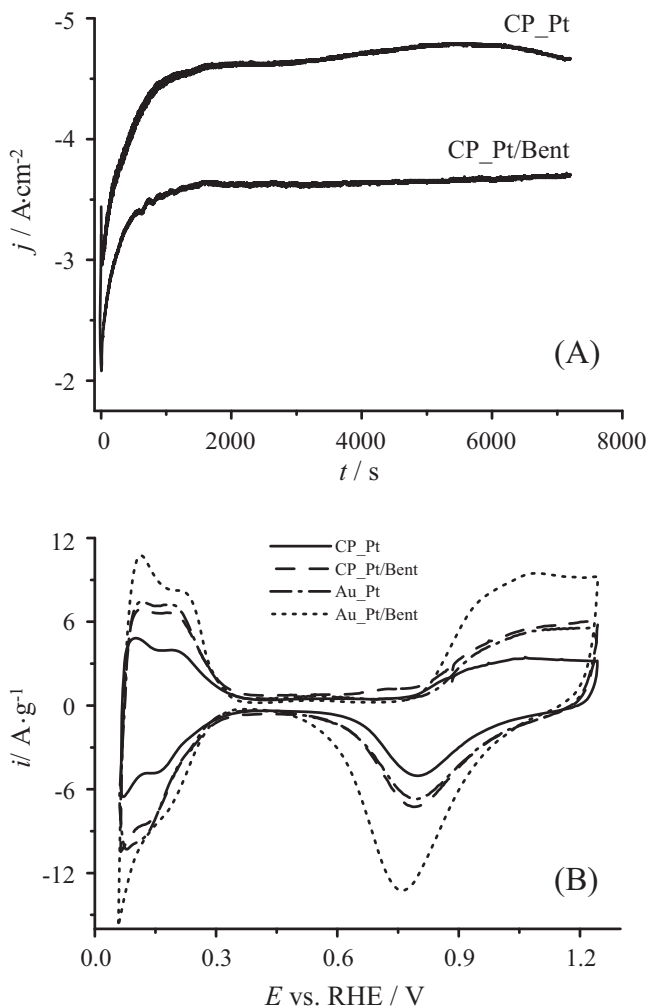


**Fig. 10.** Deposition transients (A) measured on CP electrode in 0.01 M Na<sub>2</sub>PtCl<sub>6</sub> + 0.02 M HCl solution (CP.Pt) and in clay suspensions in this solution (CP.Pt/Bent); CVs (B) of thus obtained samples (CVs for Pt and Pt/Bent deposited on Au are shown for comparison). Deposition currents are normalized per mass of the deposits.

boundaries play a major role here [61]. The sizes of the Pt particles, even being slightly different for various samples, can be hardly considered as a factor affecting the activity, because they lie beyond the range where pronounced size effects are expected.

In contrast to usual Pt deposits, for clay-templated Pt the bifunctionality can be considered as a reason of the increased activity. According to Ref. [62], Pt catalysts supported on zeolite exhibit higher electrocatalytic activity towards methanol oxidation in the range of potentials from ~270 to ~640 mV in comparison with Pt supported on carbon. Faster oxidation in the presence of zeolites was explained by the interaction of CO adsorbed on platinum with hydroxyls at the zeolites surface. This assumption is in agreement with the previously known fact [63,64] that the exchangeable cations, silanols and the Lewis acid centers of zeolites can serve as CO bonding sites. Since the interfacial chemistry of smectite clays and zeolites is rather similar, one can speculate that at not-too-low potentials the higher electrocatalytic activity of Pt/clay samples in comparison to Pt samples results from the interaction of CO with the OH-groups of clay. The enhanced electrocatalytic activity can be also a result of a weaker self-inhibition by products of strong methanol chemisorption in the presence of clay ("third-body effect"). However, a true evidence of this bifunctionality requires further efforts to characterize the location and content of clay in templated deposits.

Formally determined Tafel slopes of the steady-state methanol oxidation curves for platinized platinum of high roughness are known to be ca. 65–70 mV in the potential range under study (540–640 mV) [65]. For thinner deposits of platinum on Au ( $E_d = 100\text{--}400\text{ mV}$ ), these slopes were found to be 65–85 mV [61]. The Tafel slopes for Pt/clay on Au (Fig. 11A) are 80–95 mV, as esti-

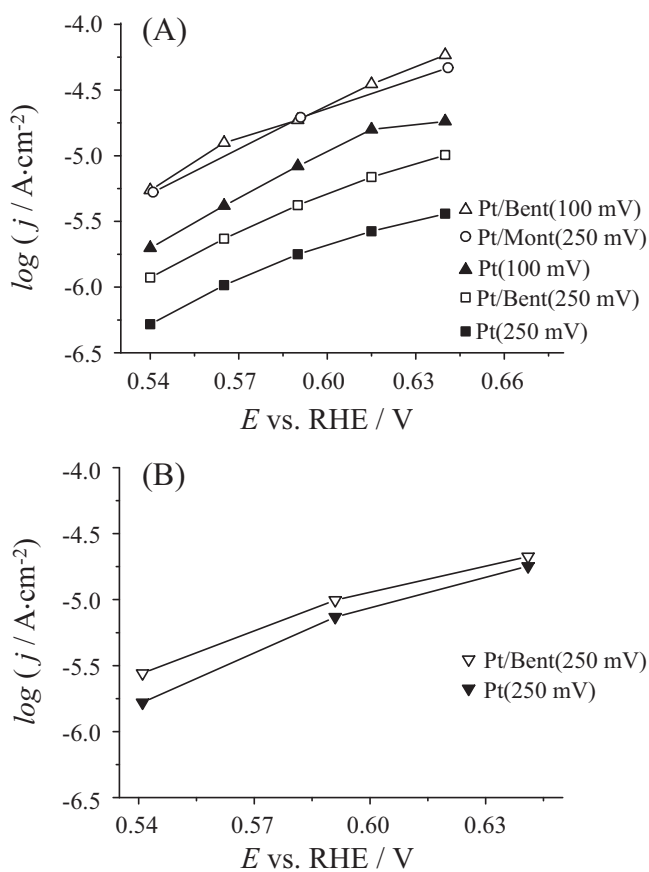


**Fig. 11.** Fragments of steady-state polarization curves of Pt and Pt/clay samples deposited on Au (A) and on CP (B). Current densities per true surface area are presented. Deposition potential (mV vs. RHE) is indicated in parentheses.

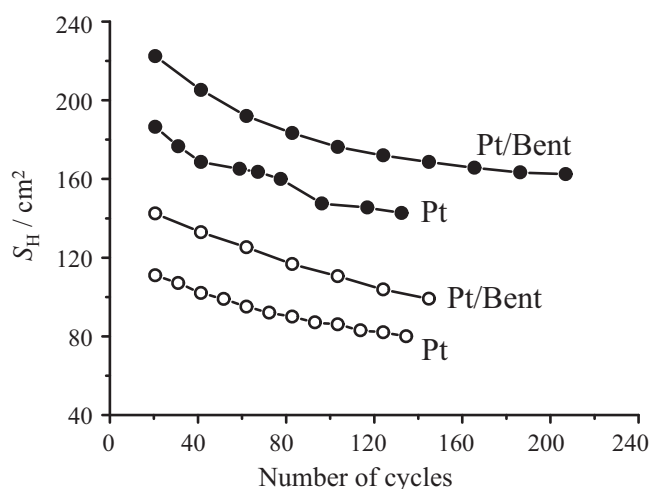


**Fig. 12.** Decrease in the true surface areas  $S_H$  of Pt and Pt/Bent samples deposited on Au (open symbols) and on CP (filled symbols) in the course of cycling ( $N$ , number of cycles).  $E_d = 250\text{ mV}$ . Total charge spent for electrodeposition of Pt and Pt/Bent samples on CP was 23 and 17 correspondingly.

ated for the potential range from 540 to 590 mV. This difference is hardly sufficient to assume changes in the catalysis mechanisms and can be attributed to the reduction of oxygen traces, being higher for thinner electrodes.

To check the stability of the Pt/Bent material under polarization in electrolyte solution, we arranged ageing tests like described in [2,6] (under a potential cycling). The decrease in the Pt true surface area with the number of cycles occurs with the same rate for all samples under study (Fig. 12). Qualitatively, it demonstrates the absence of mechanical destruction risk that could be expected because of the lower adhesion of clay-templated samples. The decay of the normalized true surface  $S_H(N)$  with the cycle number was fitted, like in Ref. [2], according to the phenomenological model of particles coalescence [66]:

$$-\frac{dS_H(N)}{dt} = \text{const} \cdot (S_H(N))^n$$

where  $n$  is a constant, independent of the thickness of the electrodeposited layer and related to the mechanism of Pt reconstruction. The value of  $n$  for the samples deposited on Au was found to be  $3.2 \pm 0.4$  for the Pt sample and  $1.8 \pm 0.2$  for the Pt/Bent sample. According to [67], this can imply different mechanisms of surface reconstruction (smoothing) for Pt and Pt/Bent: the slow surface diffusion of Pt atoms and the so-called 'atom capture', respectively. One can speculate that the higher density of dislocations and the lower content of intergrain boundaries support faster surface diffusion, but further microstructural studies are necessary in future to support this hypothesis. For samples deposited on CP, the accuracy of  $n$  determination does not allow a reliable comparison.

#### 4. Conclusions

Quasi-templating of Pt with clays results in higher true surfaces and higher specific electrocatalytic activity as compared to the pure Pt samples electrodeposited under similar mode. Taking into account the satisfactory ageing rate, these results make the new material a promising candidate for electrocatalytic applications. Clay covers a part of active nucleation centers and, therefore, (i) prevent the coalescence of Pt particles in the course of secondary nucleation; (ii) decrease the growth rate of the nuclei, supporting the formation of smaller crystals. Primary nucleation centers are also partly screened, resulting in a more poor adhesion. Organomodified smectite clay is also a promising templating

agent as soon as its organic components could provide an additional templating effect.

Two attractive properties of clays should be mentioned. First, clay particles are negatively charged, and one can easily influence the templating process by varying the deposition potential, as we demonstrated by an example of  $E_d = 100$  and  $E_d = 250$  mV. Second, the clay itself, even if trapped inside the Pt deposit, does not affect the adsorption properties or even enhances electrocatalysis. We have not observed the pronounced spillover effects known for other Pt/oxide systems, as the ratio of charges in hydrogen and oxygen regions was close to usual, but a possibility of spillover-like behavior should be taken into account in future studies of the increased catalytic activity.

Thus, quasi-templating with clay can be considered as a simple method of increasing the electrocatalytic activity of Pt catalyst. The estimation of the most important practical characteristic of catalyst (the activity per Pt mass) shows that it can be increased by a factor of 4. Quasi-templating with clay supplements our recent approach to use solid alumina template [66] and demonstrates the variety of advantages of inorganic templates for electrocatalytic applications.

## Acknowledgements

This study is supported by the Russian Foundation for Basic Researches (RFBR), project No. 08-03-00854-a and by projects RFBR No. 07-03-91583 – ASP 01-360. The authors are grateful to M.Gallyamov for helpful discussions, and also to O. Polyakova, A. Filatov and M. Kirikova for their kind help in specimen characterization.

## References

- [1] O.A. Petrii, G.A. Tsirlina, S.N. Pron'kin, F.M. Spiridonov, M.L. Khrusheva, *Rus. J. Electrochem.* 35 (1999) 8.
- [2] S.N. Pron'kin, O.A. Petrii, G.A. Tsirlina, D.J. Schiffrin, *J. Electroanal. Chem.* 480 (2000) 112.
- [3] F.J.R. Nietro, M.A. Pasquale, C.R. Carbera, A.J. Arvia, *Langmuir* 22 (2006) 10472.
- [4] L.M. Plyasova, I.Y. Molina, S.V. Cherepanova, N.A. Rudina, O.V. Sherstyuk, E.R. Savinova, S.N. Pron'kin, G.A. Tsirlina, *Rus. J. Electrochem.* 38 (2002) 1116.
- [5] L.M. Plyasova, I.Y. Molina, A.N. Gavrilov, S.V. Cherepanova, O.V. Cherstiouk, N.A. Rudina, E.R. Savinova, G.A. Tsirlina, *Electrochim. Acta* 51 (2006) 4477.
- [6] A.N. Gavrilov, O.A. Petrii, A.A. Mukovnin, N.V. Smirnova, T.V. Levchenko, G.A. Tsirlina, *Electrochim. Acta* 52 (2007) 2775.
- [7] G.A. Tsirlina, O.A. Petrii, T.Y. Safonova, I.M. Papisov, S.Y. Vassiliev, A.E. Gabrielov, *Electrochim. Acta* 47 (2002) 3749.
- [8] T.Y. Safonova, D.R. Khairullin, G.A. Tsirlina, O.A. Petrii, S.Y. Vassiliev, *Electrochim. Acta* 50 (2005) 4752.
- [9] M.I. Borzenko, M. Chojak, P. Kulesza, G.A. Tsirlina, O.A. Petrii, *Electrochim. Acta* 48 (2003) 3797.
- [10] M. Musiani, *Electrochim. Acta* 45 (2000) 3397.
- [11] A. Hovestad, L.J.J. Jansen, *J. Appl. Electrochem.* 25 (1995) 519.
- [12] R.A. Horch, T.D. Golden, A. D'Souza, L. Riestler, *Chem. Mater.* 14 (2002) 3531.
- [13] F. Uddin-Chishty, J. Orrin, A.F. Averill, *Plat. Surf. Finish.* 89 (2002) 56.
- [14] L.H. Abuhassan, M.H. Nayfeh, *Mater. Res. Soc. Symp. Proc.* 862 (2005) 301.
- [15] D.N. Pal, D. Chakravorty, *J. Phys. Chem. B* 110 (2006) 20917.
- [16] K. Momma, F. Izumi, *J. Appl. Cryst.* 41 (2008) 653.
- [17] H.H. Murray, *Appl. Clay Sci.* 5 (1991) 379.
- [18] K.E. Creasy, B.R. Shaw, *Electrochim. Acta* 33 (1998) 551.
- [19] T.J. Pinnavaia, *Science* 220 (1983) 365.
- [20] G. Szollosi, B. Toroky, L. Baranyi, M. Bartok, *J. Catal.* 179 (1998) 619.
- [21] I. Kun, G. Szollosi, M. Bartok, *J. Mol. Catal. A* 169 (2001) 235.
- [22] F.C.A. Figueiredo, E. Jordao, E. Carvalho, *Appl. Catal. A* 351 (2008) 259.
- [23] J.M. Adams, *Appl. Clay. Sci.* 2 (1987) 309.
- [24] P. Ravindranathan, P.B. Malla, S. Komarneni, R. Roy, *Catal. Lett.* 6 (1990) 401.
- [25] A. Fitch, *Clay Clay Miner.* 38 (1990) 391.
- [26] S.M. Macha, A. Fitch, *Microchim. Acta* 128 (1998) 1.
- [27] A. Walcarius, *Electroanalysis* 8 (1996) 971.
- [28] C. Senaratne, M.D. Baker, *J. Phys. Chem.* 98 (1994) 13687.
- [29] U. Hofman, *Angew. Chem.* 80 (1968) 736.
- [30] M. Alexandre, P. Dubois, *Mater. Sci. Eng.* 28 (2000) 1.
- [31] S.G. Starodoubtsev, E.K. Lavrentyeva, A.R. Khokhlov, G. Allegra, A. Famulari, S.V. Meille, *Langmuir* 22 (2006) 369.
- [32] N.M. Nagy, J. Konya, M. Foldvari, P. Kovacs-Palfly, *Czech. J. Phys.* 53 (2003) A103.
- [33] ICDD, PDF2. <http://www.icdd.com/products/pdf2.htm>, 2011.
- [34] P. Scardi, M. Leoni, *Acta Cryst.* A58 (2002) 190–200.
- [35] M. Leoni, T. Confente, P. Scardi, Z. Kristallogr. Suppl. 23 (2006) 249–254.
- [36] D.M. Moore, R.C. Reynolds Jr., *X-ray Diffraction and the Identification and Analysis of Clay Minerals*, Oxford University Press, New York, 1989.
- [37] S.Y. Vassiliev, A.V. Denisov, *Zh. Tekhn. Fiziki* 70 (2000) 100.
- [38] A.I. Yusipovich, S.Y. Vassiliev, *Rus. J. Electrochem.* 41 (2005) 510.
- [39] S. Choi, G. Crosson, K.T. Mueller, S. Seraphin, J. Chorover, *Geochim. Cosmochim. Acta* 69 (2005) 4437.
- [40] T. Nagashi, M. Akizuki, *Canad. Miner.* 35 (1997) 947.
- [41] A. Frumkin, B. Damaskin, N. Grigoryev, I. Bagotskaya, *Electrochim. Acta* 19 (1974) 69.
- [42] A.N. Frumkin, O.A. Petry, *Electrochim. Acta* 15 (1970) 391.
- [43] R.F. Giese, C.J. Van Oss, *Colloid and Surface Properties of Clays and Related Minerals*, Marcel Dekker Inc., New York, 2002.
- [44] M. Chorom, P. Rengasamy, *Eur. J. Soil Sci.* 46 (1995) 657.
- [45] O. Duman, S. Tunk, *Micropor. Mesopor. Mater.* 117 (2009) 331.
- [46] G.S. Attard, P.N. Bartlett, N.R.B. Coleman, J.M. Elliott, J.R. Owen, J.H. Wang, *Science* 278 (1997) 838.
- [47] G.S. Attard, C.G. Goltner, J.M. Corker, S. Henke, R.H. Templer, *Angew. Chem. Int. Ed.* 36 (1997) 1315.
- [48] A.P. Silva, S.S. Marqueti, G. Maia, *ECS Trans.* 3 (2007) 9.
- [49] E. Bahena, P.F. Mendez, Y. Meas, R. Ortega, L. Saldago, G. Trejo, *Electrochim. Acta* 49 (2004) 989.
- [50] S.N. Pron'kin, G.A. Tsirlina, O.A. Petrii, S.Y. Vassiliev, *Electrochim. Acta* 46 (2001) 2343.
- [51] C. Song, G. Villemure, *J. Electroanal. Chem.* 462 (1999) 143.
- [52] W. Klaus, G. Nolze, *J. Appl. Cryst.* 29 (1996) 301.
- [53] R. Jenkins, R.L. Snyder, *Introduction to X-Ray Powder Diffractometry*, John Wiley & Sons, Inc., New York/Chichester/Brisbane/Toronto/Singapore, 1996.
- [54] P. Scardi, M. Leoni, *Acta Cryst.* A57 (2001) 604.
- [55] J. Gubicza, T. Ungar, Z. Kristallogr. 222 (2007) 567.
- [56] D. Tromans, J.A. Meech, *Mater. Eng.* 14 (2001) 1359.
- [57] J.D. Lovic, A.V. Tripkovic, S.L. Gojkovic, K.D. Popovic, D.V. Tripkovic, P. Olszewski, A. Kowal, *J. Electroanal. Chem.* 581 (2005) 294.
- [58] P.V. Samant, C.M. Rangel, M.H. Romero, J.B. Fernandes, J.L. Figueiredo, *J. Power Sources* 151 (2005) 79.
- [59] A. Pozio, M.D. Francesco, A. Cemmi, F. Cardellini, L. Giorgi, *J. Power Sources* 105 (2002) 13.
- [60] F. Gloaguen, J.M. Leger, C. Lamy, A. Marmann, U. Stimming, R. Vogel, *Electrochim. Acta* 44 (1999) 1805.
- [61] O.V. Cherstiouk, A.N. Gavrilov, L.M. Plyasova, I.Y. Molina, G.A. Tsirlina, E.R. Savinova, *J. Solid State Electrochem.* 12 (2008) 497.
- [62] P.V. Samant, J.B. Fernandes, *J. Power Sources* 125 (2004) 172.
- [63] B.S. Shete, V.S. Kamble, N.M. Gupta, V.B. Kartha, *J. Phys. Chem. B* 102 (1998) 5581.
- [64] V.S. Kamble, N.M. Gupta, *J. Phys. Chem. B* 104 (2000) 4588.
- [65] O.A. Petry, B.I. Podlovchenko, A.N. Frumkin, H. Lal, *J. Electroanal. Chem.* 10 (1965) 263.
- [66] K.S. Napolskii, P.J. Barczuk, S.Y. Vassiliev, A.G. Veresov, G.A. Tsirlina, P.J. Kulesza, *Electrochim. Acta* 52 (2007) 7910.
- [67] E. Ruckenstein, B. Pulvermacher, *J. Catal.* 29 (1973) 224.